

On the bad metallicity and phase diagrams of $\text{Fe}_{1+\delta}X$ ($X=\text{Te, Se, S}$, solid solutions): an electrical resistivity study

M. ElMassalami,¹ K. Deguchi,² T. Machida,³ H. Takeya,² and Y. Takano²

¹*Instituto de Física, Universidade Federal do Rio de Janeiro,
Caixa Postal 68528, 21941-972 Rio de Janeiro RJ, Brazil*

²*National Institute for Materials Science, 1-2-1, Sengen, Tsukuba, 305-0047, Japan*

³*Department of Physics, Tokyo University of Science,
1-3 Kagurazaka, Shinjuku-ku, Tokyo 162-8601, Japan*

(Dated: October 13, 2014)

Based on a systematic analysis of the thermal evolution of the resistivities of Fe-based chalcogenides $\text{Fe}_{1+\delta}\text{Te}_{1-x}\text{X}_x$ ($X=\text{Se, S}$), it is inferred that their often observed nonmetallic resistivities are related to a presence of two resistive channels: one is a high-temperature thermally-activated process while the other is a low-temperature log-in- T process. On lowering temperature, there are often two metal-to-nonmetal crossover events: one from the high- T thermally-activated nonmetallic regime into a metal-like phase and the other from the log-in- T regime into a second metal-like phase. Based on these events, together with the magnetic and superconducting transitions, a phase diagram is constructed for each series. We discuss the origin of both processes as well as the associated crossover events. We also discuss how these resistive processes are being influenced by pressure, intercalation, disorder, doping, or sample condition and, in turn, how these modifications are shaping the associated phase diagrams.

I. INTRODUCTION

It is remarkable that the normal-state resistivities of $\text{Fe}_{1+\delta}X$ ($X=\text{Te, Se, S}$, or their solid solutions)¹⁻⁴ as well as those of intercalated $A_x\text{Fe}_{2-y}\text{Se}_2$ ($A=\text{K, Rb, Cs, Tl, ...}$)⁵⁻⁷ are neither truly metallic nor truly insulating. It is also remarkable that the normal-state and superconducting phase diagrams of these chalcogenides are highly irreproducible and markedly different from one another. In fact, reported resistivities of the very same stoichiometric compound do not show the same thermal/magnetic/baric/concentration evolution, $\rho(T, H, P, x)$, or the same crossover/transition events. It is then no surprise that these phase diagrams (being constructed out of such characterization) manifest a strong dependence on sample condition or history.¹⁻⁴

Although an earlier electronic structure calculations predicted a low-carrier-density metallic character,⁸ the isomorphous $\text{Fe}_{1+\delta}X$ compounds exhibit a variety of normal-state behavior: $\text{Fe}_{1+\delta}\text{S}$ is nonmetallic below $T_{MNM} \sim 300$ K [Ref.9] but T_{MNM} can be strongly reduced by pressure.¹⁰ $\text{Fe}_{1+\delta}\text{Se}$ is a nonmagnetic metal, undergoes a structural phase transition at $T_S \sim 90$ K, and superconducts at $T_c \sim 8$ K.¹¹ Finally, $\text{Fe}_{1+\delta}\text{Te}$ is a nonmetallic paramagnet above a magnetic and structural transition at $T_{MS} \sim 70$ K while a metallic antiferromagnet (AFM) below T_{MS} .^{12,13}

In this work we address the above mentioned bad metallicity of $\text{Fe}_{1+\delta}\text{X}_{1-x}\text{Y}_x$ chalcogenides. Based on the analysis of their resistivities and on the obtained phase diagrams, we identified two processes that are responsible for their bad metallic character as well as for shaping their phase diagrams: the first is a high-temperature (150 to 300 K) thermally-activated process¹⁴ while the other is a low-temperature (< 100 K) log-in- T process.¹⁵

II. GUIDELINES FOR ANALYZING $\rho(T, P, x)$

In order to rationalize the variety of functional forms of $\rho(T, P, x)$ and, in addition, so as to identify and evaluate the strength of the involved resistive channels, let us assume, based on earlier studies,¹⁶⁻¹⁹ that the character of their normal-state is shaped by the combined influences of crystalline electric field interactions, electronic correlations, disorder, and band filling: based on the strength of these factors, the high-temperature ($T > 100$ K) normal state could be either metallic, Mott insulator, or an intermediate orbital-selective Mott phase (OSMP) wherein some of the Fe $3d$ orbitals are localized while the others are itinerant.^{14,16-19} The high- T phase of most of the studied intercalated $A_x\text{Fe}_{2-y}\text{Se}_2$ (as well as most of $\text{Fe}_{1+\delta}\text{X}_{1-x}\text{Y}_x$, see below) compounds is reported to be an OSMP.^{14,16-19} We assumed that, within this OSMP, localized states are separated from itinerant ones by a mobility edge at E_c .²⁰ Then the thermal evolution of the resistivity depends on the relative strength of $|E_c - E_F|$ with respect to $k_B T$: if E_c is not located in the $3d$ multiplet or that $|E_c - E_F| > k_B T$, then transport is effected by a thermally-assisted hopping among the localized orbitals leading to a Mott variable range hopping resistivity (VRH):

$$\rho(T) = \rho_0^{vrh} \exp([T_{vrh}/T]^{\frac{1}{d+1}}), \quad (1)$$

where $d=2$ (3) represents a 2- (3-) dimensionality and all other terms have their usual meaning. If $|E_c - E_F| < k_B T$, as assumed for the under-study Fe-based compounds, then $\rho(T)$ is governed by the Arrhenius process:²¹

$$\rho(T) = \rho_0^A \exp(|E_c - E_F|/T) = \rho_0^A \exp(\Delta/T). \quad (2)$$

Previous studies on these OSMPs reported that, due to the characteristic arrangement of the energy levels

of the involved Fe-3d-orbitals as well as due to entropy arguments, a lowering of temperature often leads to a temperature-induced crossover (OSMT) from an OSMF into a metallic phase at T_X^{HT} .^{14,16}

In addition to the activated high-temperature process, the low temperature resistivities of various chalcogenides^{3,22,23} are reported to exhibit another process which, in most cases, can be approximated as a log-in- T contribution:

$$\rho(T) = \rho_o^{LT} [1 + S \ln(T_o/T)], \quad (3)$$

the logarithmic slope S is a measure of the intensity of the process while T_o and ρ_o^{LT} are characteristic, here experimentally-determined, parameters. In contrast to the activated process, the origin of such a log-in- T behavior is not well studied; as such this will be discussed below after the analysis of our results.

Depending on the relative strength of the above-mentioned two resistive channels, $\rho(T)$ would assume a variety of functional forms: $\frac{\partial \rho}{\partial T}$ would be positive for a metallic character while negative for any nonmetallic contribution.^{24,25} In addition, $\frac{\partial \rho}{\partial T}$ would be helpful in identifying transition/crossover events (e.g. a metal-to-nonmetal, MNM , crossover is manifested as a maximum in the resistivity: $\frac{\partial \rho}{\partial T} = 0$). In general, on cooling, two crossovers may be observed: one from the high- T activated regime into a metal-like phase (metal-I) at T_X^{HT} and another from the low- T log-in- T regime into a metal-like phase (metal-II) at T_X^{LT} (see below); it is emphasized that, for $\text{Fe}_{1+\delta}(\text{Te}_{1-x}\text{Se}_x)$ $0.1 \leq x \leq 0.5$, both T_X^{LT} and T_X^{HT} events (see also Refs. 3, 26, and 27) are not accompanied by any visible symmetry-breaking process.

III. RESULTS

Samples preparation, annealing, and measurements (namely structural, elemental, magnetization and resistivity) of $\text{FeTe}_{1-x}\text{Se}_x$ and $\text{FeTe}_{1-x}\text{S}_x$ series were the same as the ones reported in previous works.²⁸ The above-mentioned resistivity analysis was applied to the measured curves of these samples: this analysis can be readily extended to other chalcogenides.

Figure 1 show $\rho(T)$ curves of two, representatives, oxygen-annealed $\text{FeTe}_{1-x}\text{Se}_x$ samples. A closer look at Fig. 1(b) reveals that $\frac{\partial \rho_n}{\partial T}$ ($45 < T < 300\text{K}$) exhibits, approximately, two negative values; each is taken to indicate a distinct resistive channel, stemming from a distinct origin, operating within a distinct temperature region, and has a distinct thermal evolution: the one operating within $150 < T < 300\text{K}$ is an activated process (see above) while the other, operating below 100K , is a log-in- T process.

The thermal evolution of the activated process is exhibited in Figs. 1(d, h). In spite of the polycrystalline form and the limited temperature range available for this behavior, a fit $\rho(250 < T < 300\text{K})$ to Eq. 1 [see Fig. 1(h)]

indicates a simple Arrhenius expression of Eq. 2 wherein the effective single parameter Δ is taken to represent a mean localization energy separating the Fermi level from the closest mobility edge.²¹ For the particular case of $\text{FeTe}_{1-x}\text{Se}_x$, this $\Delta \sim 40\text{K}$ is, roughly, the same for all x [see Fig. 2(c)]: such a Δ should not be confused with that of an activated semiconductivity.

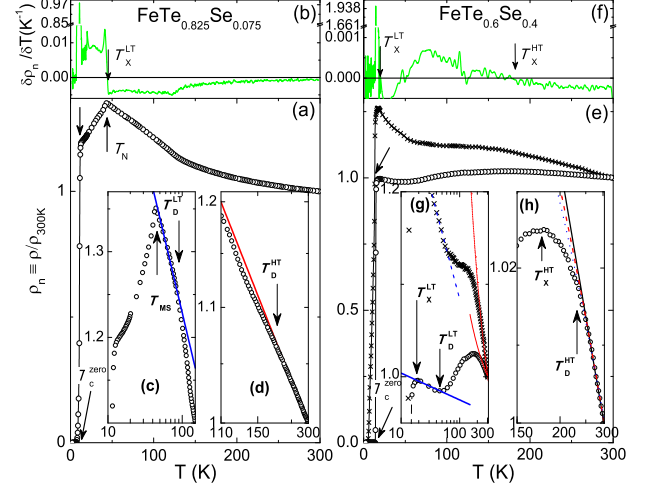


FIG. 1. Normalized $\rho_n \equiv \rho/\rho_{300\text{K}}$ curves of $\text{FeTe}_{0.925}\text{Se}_{0.075}$ (a-d) and $\text{FeTe}_{0.6}\text{Se}_{0.4}$ (e-h). (a, e) ρ_n vs T curves. (b, f) $\frac{\partial \rho_n}{\partial T}$ vs T curves showing the crossover at T_X^{LT} and T_X^{HT} whereat $\frac{\partial \rho_n}{\partial T} = 0$. (c, g) ρ_n vs T curves in a linear-log plot. The solid lines is a fit to Eq. 3. $S(x)$ is shown in Fig. 2(c). (d, h) ρ_n vs T curves in a log-reciprocal plot. The solid, dashed and dotted lines are, resp., a fit to Eq. 2, Eq. 1 ($d=2$) and Eq. 1 ($d=3$). Notice that T_D^{HT} is the lower point at which $\rho_n(T)$ starts to deviate away from Eq. 2 while T_D^{LT} is the upper deviation point from Eq. 3. The cross symbols in (e) and (g) represent the resistivity of the as-prepared sample: annealing in O_2 reduces the two resistive contributions (also evident in e.g. Ref. 29) [here $S_{\text{as-prep}} = 0.089(3)$ while $S_{\text{O}_2} = 0.013(1)$].

On the other hand, Figs. 1(c, g) indicates that $\rho(T_X^{LT} < T < T_D^{LT})$ follows Eq. 3,^{22,30} wherein S , the only fit parameter, is shown in Fig. 2 (c).

In addition to the manifestation of two resistive channels, $\rho(T, x)$ of $\text{FeTe}_{1-x}\text{Se}_x$ show some other finer details: (i) $\rho(T, x < 0.1)$ curves are different from the ones with $0.1 \leq x \leq 0.5$: the dividing line, $x \sim 0.1$, coincides with the concentration beyond which the magnetism is suppressed.¹⁻³ (ii) $\rho(T, x < 0.1)$ starts to deviate away from Eq. 2 at T_D^{HT} ; on further cooling, $\rho(T, x < 0.1)$ exhibits a sharp drop at $T_{MS}(x)$ (related to the reported magnetic and structural transition³¹) followed by a metallic behavior. On cooling well below T_{MS} , $\rho(T < T_{MS}, x < 0.1)$ exhibits the transitions associated with weak and bulk superconductivity.^{1,2} (iii) $\rho(T, 0.1 \leq x \leq 0.5)$ exhibits also a deviation from Eq. 2 at T_D^{HT} , followed by a crossover into a metallic state at $T_X^{HT}(x)$ [see Fig. 1(f)]. On further cooling, the resistivity once more exhibits the log-in- T behavior, a crossover into a metallic state at $T_X^{LT}(x)$, and finally, the bulk su-

perconductivity at T_c^{zero} .

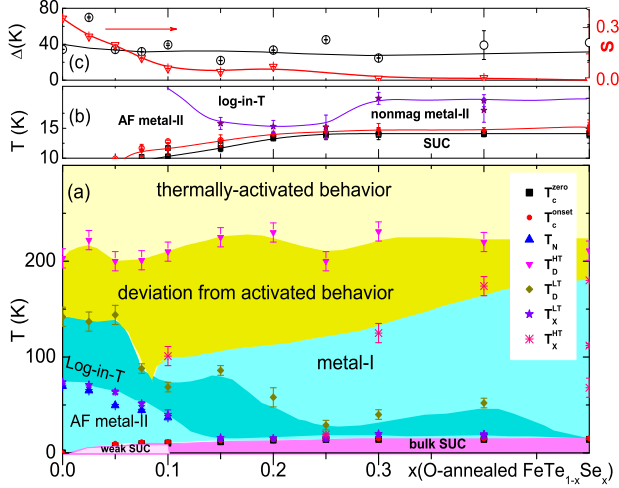


FIG. 2. (a) A phase diagram of $\text{FeTe}_{1-x}\text{Se}_x$ ($0 \leq x \leq 0.5$, annealed in O_2). (b) The x -dependence of the closely-spaced T_c^{zero} , T_c^{onset} and T_X^{LT} events: in spite of their closeness, the metallic state is (re)established well before the onset of superconductivity. (c) *Left ordinate*: Δ versus x (the determination of Δ and T_{VRH} is strongly influenced by the choice among Eqs.1 or 2 and among the limits of the available T -range). *Right ordinate*: the logarithmic slope $S(x)$ as obtained from the fit of Eq. 3.

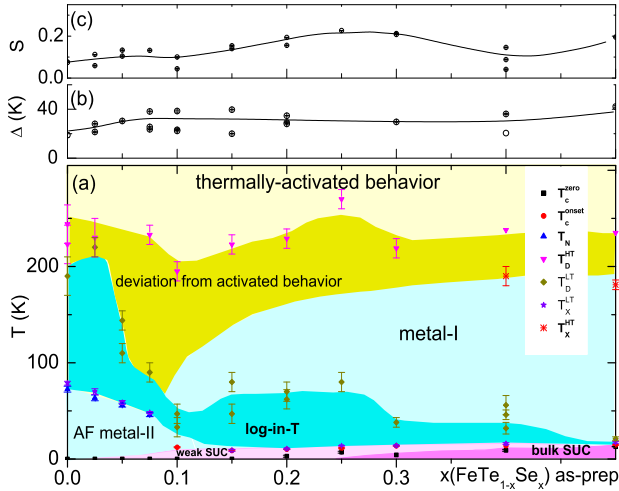


FIG. 3. (a) The phase diagram of as-prepared $\text{FeTe}_{1-x}\text{Se}_x$ ($0 \leq x \leq 0.5$). The difference between this diagram and that of oxygen-annealed one (Fig. 2) emphasizes the role of annealing and oxygen intercalation in shaping the normal and superconducting states of these chalcogenides. (b) Effective Δ versus x as obtained from the fit of Eq.2 within $250 \leq T \leq 300$ K. (c) S versus x as obtained from the fit of Eq. 3.

All the above-mentioned resistivity events of oxygen-annealed $\text{FeTe}_{1-x}\text{Se}_x$ samples are collected in Fig. 2: in addition to the transitions at T_{MS} and T_c^{zero} and the crossovers at T_X^{HT} and T_X^{LT} , we also include T_D^{HT} and

T_D^{LT} . Similar analyses were carried out on the resistivities of as-prepared $\text{FeTe}_{1-x}\text{Se}_x$ samples as well as those of $\text{FeTe}_{0.8}\text{S}_{0.2}$ (representative of $\text{FeTe}_{1-x}\text{Se}_x$): the obtained phase diagrams are shown, respectively, in Figs. 3 and 4.

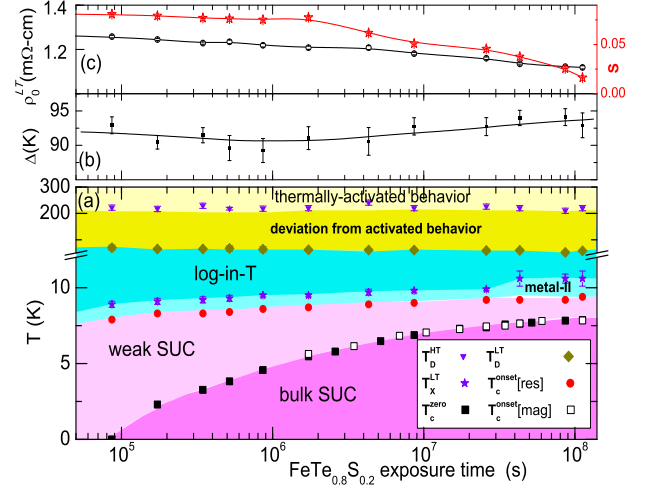


FIG. 4. (a) The time evolution of the superconducting, magnetic and transport properties of as-prepared $\text{FeTe}_{0.8}\text{S}_{0.2}$. The resistivities and magnetizations (see Fig. 11 in Ref. 2) were measured at the plotted time intervals while the sample was being continuously exposed to air at ambient temperature. Similar phase diagrams can be obtained for other intercalation processes. (b) Effective Δ versus x as obtained from the fit of Eq.2 within $250 \leq T \leq 300$ K. (c) the evolution of ρ_o^{LT} (left ordinate) and S (right ordinate) versus x as obtained from the fit of Eq. 3.

The pressure influence on the superconducting and normal-state properties of these chalcogenides was extensively studied [see e.g., $\text{Fe}_{1+\delta}\text{Te}$,³² $\text{Fe}_{1+\delta}\text{Se}$,^{33–39} $\text{Fe}_{1+\delta}\text{S}$,¹⁰ and $\text{Fe}_{1+\delta}(\text{Te}_{1-x}\text{Se}_x)$.^{40–43}] In general, $\rho(T_c < T < 300\text{K})$ is strongly reduced by P . It is noticed that, even for pressures leading to amorphization,⁴³ the evolution of $\rho(T_c < T < 300\text{K}, P)$ does not support an interpretation in terms of a closure of a semiconducting gap. Rather, such an influence can be envisaged as a reduction of the two resistive channels and an enhancement of the metallic state: For $\text{Fe}_{1+\delta}\text{Te}$, the metallic state (stabilized below T_{MS} at ambient pressure) is enhanced to ~ 240 K at 7 GPa,³² while for $\text{Fe}_{1+\delta}\text{Se}$, the metallic state (stabilized above 300 K at ambient pressure) is extended downwards to ~ 70 K at ~ 3 GPa.¹⁰

Finally, $T_{N,mag}$ and $T_{c,mag}^{onset}$, as determined from magnetization curves (not shown), are shown in the respective phase diagrams; evidently $T_{c,mag}^{onset}$ equals $T_{c,\rho}^{zero}$; as such $T_{c,\rho}^{onset}$ should not be taken as an onset of superconductivity, rather it is $\sim T_X^{LT}$ (see below).

IV. DISCUSSION AND CONCLUSIONS

We showed a consistent and a unified analysis of $\rho(x, P, T < 300\text{K})$ based on consideration of an activated and a log-in- T processes. Various x -dependent transition/crossover events (T_{MS} , T_N , T_c^{zero} , T_X^{HT} , T_X^{LT} , T_D^{HT} and T_D^{LT}) were identified and these points were used to construct the corresponding x - T phase diagrams; that these diagrams are topologically equivalent to the earlier reported ones^{1-4,31,44-46} emphasizes the role of these channels in shaping the phase diagrams.

The origin of the high- T activated process, as already discussed, is related to the presence of an orbital-selective Mott phase.^{14,16-19} A careful analysis of this process in $\text{Fe}_{1+\delta}\text{X}$ suggests that $\text{Fe}_{1+\delta}\text{S}$ is at the vicinity of Mott transition, $\text{Fe}_{1+\delta}\text{Se}$ is at a metallic side, while $\text{Fe}_{1+\delta}\text{Te}$ and $\text{Fe}_{1+\delta}\text{Te}_{1-x}\text{Y}_x$ solid solutions are at an intermediate orbital-selective Mott phase. A variation in any of the control parameters (crystal structure, intercalation, pressure, defects, or filling) would turn the normal-state into either a metal-like, an activated OSMP, or a Mott insulator.^{7,14,16-19} This was elegantly illustrated in the case of $\text{AFe}_{2-y}\text{Se}_2$.^{6,14}

The origin of the low- T localization, on the other hand, can be deduced from the scanning tunneling microscopy studies of Machida *et al.*⁴⁷ which revealed (at 4.2 K, within the metallic state of $\text{Fe}_{1+\delta}\text{Te}$) the presence of an inhomogeneous distribution of local density of states (LDOS) around the randomly-distributed defect centres (suggested to be excess Fe): LDOS is increased around these centres while depleted away from them. Scattering from such nonperiodic potentials is assumed to be the cause of the low- T process.^{3,22,23,48,49} Indeed, the strength of such a process is strongly controlled by the concentration of defects: this is well illustrated in the correlation of $\rho(T < T_{MS})$ with δ in $\text{Fe}_{1+\delta}\text{Te}$ [48] as well as in the correlation of $S(x)$ (see Fig. 2) with the excess Fe or chalcogen deficiency.²⁹ In general, the control of scattering centres can be effected by annealing (Fig. 2 and Ref. 50), applying pressure (Refs.10, 32-43), or intercalation (Fig. 4 and Ref. 2).

This defect-driven low- T process is manifested here as, though not limited to, a log-in- T term; three possible mechanisms can be suggested for this log-in- T behavior: (i) a typical Kondo or any of the formally analogous processes arising from scattering against nonmagnetic degenerate-state impurities,^{51,52} (ii) Anderson weak localization wherein defects lead to a coherent backscattering of non-interacting electrons,^{53,54} or (iii) Altshuller-Aronov¹⁵ weak localization wherein the system of interacting electrons are subjected to a random potential. The following considerations elect the Altshuller-Aronov weak localization process: First, these chalcogenides are structurally formed from Fe_2X_2 layers that are coupled to their neighbors by weak van der Waals forces. Second, the observation of stronger correlation

effects in chalcogenides⁸ suggests a scenario of *interacting* electrons in a random potential which may arise from a randomly-distributed (paramagnetic and/or nonmagnetic) impurities.

The identification of the origins of these two processes makes it easy to trace down the influence of perturbations (such as pressure, intercalation, annealing, ..) on the boundary lines at T_X^{LT} and T_X^{HT} of the studied phase diagrams. While the origin of the crossover at T_X^{HT} is already discussed, that of T_X^{LT} is most probably related to the fluctuation-induced formation of incoherent Cooper pairs which is favored by disorder and lower dimensionality of chalcogenides.^{55,56} due to the onset of these fluctuations, the metallic-like character is (re)established well before the onset of superconductivity (see Figs. 2, 3, 4). This feature is reminiscent of the situation in both nonconventional underdoped HT_c , see e.g. Ref. 24, and conventional LT_c superconductors.⁵⁵ Accordingly, T_X^{LT} may be identified as the onset point, T^* , of a pseudogap phase.³⁰ It is emphasized that this low-temperature disorder-driven metal-nonmetal transition is different from the high-temperature Mott metal-nonmetal transition.

The competition between superconductivity and localization, observed above, may be discussed in terms of a competition between an attractive (V_p) and a repulsive (V_c) interactions. On assuming an effective coupling $\lambda_{eff} = \lambda - \mu^*$ wherein $\lambda = V_p N_{EF}$ and $\mu^* = \frac{V_c N_{EF}}{1 + V_c N_{EF} \ln(\frac{\omega_c}{\omega_D})}$ (all terms have their usual meaning),⁵⁷ then (i) an increase in, say, disorder would augment μ^* which, being in competition with superconductivity, would degrade and, above a critical value, eventually quench the superconductivity.⁵⁵ A further increase of disorder would eventually lead to a stronger Anderson-type localization as best illustrated in $\text{Fe}_{1.01-x}\text{Cu}_x\text{Se}$.⁵⁸ (ii) the manifestation of T_X^{LT} and the associated metal-II phase is conditioned by the strength of the attractive term: if no or weaker superconductivity, then no T_X^{LT} event.

Finally, based on the above-mentioned remarks, it is easy to understand (i) why the resistivity behavior of most Fe-based chalcogenides are neither truly metallic nor truly insulating, (ii) why some events are not exhibited in the reported resistivities of the as-prepared or annealed/intercalated samples, and (iii) why the reported superconducting and magnetic phase diagrams are strongly influenced by sample conditions (compare Figs. 2 and 3).

ACKNOWLEDGMENTS

We acknowledges fruitful discussions with D Edwards, N Trivedi, J Albuquerque, C M Chaves, A Troper, M A C Gusmao, L Craco, C Lewenkopf, and S Das Sarma.

- ¹ Y. Mizuguchi and Y. Takano, J. Phys. Soc. Jpn. **79**, 102001 (2010).
- ² K. Deguchi, Y. Takano, and Y. Mizuguchi, Sci. Technol. Adv. Mater. **13**, 054303 (2012).
- ³ T. J. Liu *et al.*, Nat. Mater. **9**, 716 (2010); N. Katayama, S. Ji, D. Louca, S. Lee, M. Fujita, T. J. Sato, J. Wen, Z. Xu, G. Gu, G. Xu, Z. Lin, M. Enoki, S. Chang, K. Yamada, and J. M. Tranquada, J. Phys. Soc. Jpn. **79**, 113702 (2010).
- ⁴ B. C. Sales, A. S. Sefat, M. A. McGuire, R. Y. Jin, D. Mandrus, and Y. Mozharivskyj, Phys. Rev. B **79**, 094521 (2009); M. Tropeano, I. Pallecchi, M. R. Cimberle, C. Ferdeghini, G. Lamura, M. Vignolo, A. Martinelli, A. Palenzona, and M. Putti, Supercond. Sci. Technol. **23**, 054001 (2010).
- ⁵ J. Guo, S. Jin, G. Wang, S. Wang, K. Zhu, T. Zhou, M. He, and X. Chen, Phys. Rev. B **82**, 180520 (2010).
- ⁶ M.-H. Fang, H.-D. Wang, C.-H. Dong, Z.-J. Li, C.-M. Feng, J. Chen, and H. Q. Yuan, Europhys. Lett. **94**, 27009 (2011); T. P. Ying, X. L. Chen, G. Wang, S. F. Jin, T. T. Zhou, X. F. Lai, H. Zhang, and W. Y. Wang, Nature Sci. Rep. **2**, 426 (2012); D. M. Wang, J. B. He, T.-L. Xia, and G. F. Chen, Phys. Rev. B **83**, 132502 (2011).
- ⁷ Z. Wang, M. Schmidt, J. F. V. Tsurkan, M. Greger, D. Vollhard, A. Loid, and J. Deisenhofer, Nature Commun **5**, 3202 (2014); F. Chen, M. Xu, Q. Q. Ge, Y. Zhang, Z. R. Ye, L. X. Yang, J. Jiang, B. P. Xie, R. C. Che, M. Zhang, A. F. Wang, X. H. Chen, D. W. Shen, J. P. Hu, and D. L. Feng, Phys. Rev. X **1**, 021020 (2011).
- ⁸ D. J. Singh, Sci. Technol. Adv. Mater **13**, 054304 (2012).
- ⁹ E. F. Bertaut, P. Burlet, and J. Chappert, Solid State Comm. **3**, 335 (1965).
- ¹⁰ S. Denholme *et al.*, Sci. Technol. Adv. Mater. (2014), in press.
- ¹¹ T. M. McQueen, A. J. Williams, P. W. Stephens, J. Tao, Y. Zhu, V. Ksenofontov, F. Casper, C. Felser, and R. J. Cava, Phys. Rev. Lett. **103**, 057002 (2009).
- ¹² W. Bao *et al.*, Phys. Rev. Lett. **102**, 247001 (2009).
- ¹³ S. Li, C. de la Cruz, Q. Huang, Y. Chen, J. W. Lynn, J. Hu, Y.-L. Huang, F.-C. Hsu, K.-W. Yeh, M.-K. Wu, and P. Dai, Phys. Rev. B **79**, 054503 (2009).
- ¹⁴ M. Yi, D. H. Lu, R. Yu, S. C. Riggs, J.-H. Chu, B. Lv, Z. K. Liu, M. Lu, Y.-T. Cui, M. Hashimoto, S.-K. Mo, Z. Hussain, C. W. Chu, I. R. Fisher, Q. Si, and Z.-X. Shen, Phys. Rev. Lett. **110**, 067003 (2013); P. Gao, R. Yu, L. Sun, H. Wang, Z. Wang, Q. Wu, M. Fang, G. Chen, J. Guo, C. Zhang, D. Gu, H. Tian, J. Li, J. Liu, Y. Li, X. Li, S. Jiang, K. Yang, A. Li, Q. Si, and Z. Zhao, Phys. Rev. B **89**, 094514 (2014).
- ¹⁵ B. L. Altshuler and A. G. Aronov, Solid State Commun **46**, 429 (1983).
- ¹⁶ R. Yu and Q. Si, Phys. Rev. Lett. **110**, 146402 (2013).
- ¹⁷ L. Craco, M. S. Laad, and S. Leoni, Phys. Rev. B **84**, 224520 (2011).
- ¹⁸ Z. P. Yin, K. Haule, and G. Kotliar, Phys. Rev. B **86**, 195141 (2012).
- ¹⁹ E. Bascones, B. Valenzuela, and M. J. Calderón, Phys. Rev. B **86**, 174508 (2012).
- ²⁰ N. F. Mott, J Physics C: Solid State Physics **20**, 3075 (1987).
- ²¹ D. Basko, I. Aleiner, and B. Altshuler, Annals of Physics **321**, 1126 (2006).
- ²² T. J. Liu *et al.*, Phys. Rev. B **80**, 174509 (2009).
- ²³ H. H. Chang, J. Y. Luo, C. T. Wu, F. C. Hsu, T. W. Huang, P. M. Wu, M. K. Wu, and M. J. Wang, Supercond. Sci. Technol. **25**, 035004 (2012).
- ²⁴ Y. Ando, S. Komiya, K. Segawa, S. Ono, and Y. Kurita, Phys. Rev. Lett. **93**, 267001 (2004).
- ²⁵ Y. J. Song, J. B. Hong, B. H. Min, Y. S. Kwon, K. J. Lee, M. H. Jung, and J.-S. Rhyee, J. Korean Phys.Soc. **59**, 312 (2011).
- ²⁶ Y. Liu, R. K. Kremer, and C. T. Lin, Supercond. Sci. Technol. **24**, 035012 (2011).
- ²⁷ C. S. Yadav and P. L. Paulose, J. Appl. Phys. **107**, 083908 (2010).
- ²⁸ K. Deguchi, S. Demura, T. Yamaki, H. Hara, S. Denholme, M. Fujioka, H. Okazaki, H. Takeya, and T. Y. Y. Takano, J Supercond Nov Magn **27**, 305 (2014).
- ²⁹ Y. Sun, Y. Tsuchiya, T. Taen, T. Yamada, S. Pyon, A. S. T. E. Z. Shi, and T. Tamegai, Scientific Reports **4**, 4585 (2014).
- ³⁰ I. Pallecchi, M. Tropeano, C. F. G. Lamura, A. Martinelli, A. Palenzona, and M. Putti, J Supercond Nov Mag **24**, 1751 (2011).
- ³¹ A. Martinelli, A. Palenzona, M. Tropeano, C. Ferdeghini, M. Putti, M. R. Cimberle, T. D. Nguyen, M. Affronte, and C. Ritter, Phys. Rev. B **81**, 094115 (2010).
- ³² H. Okada, H. Takahashi, Y. Mizuguchi, Y. Takano, and H. Takahashi, J. Phys. Soc. Jpn. **78**, 083709 (2009).
- ³³ Y. Mizuguchi, F. Tomioka, S. Tsuda, T. Yamaguchi, and Y. Takano, Appl. Phys. Lett. **93**, 152505 (2008).
- ³⁴ S. Margadonna, Y. Takabayashi, Y. Ohishi, Y. Mizuguchi, Y. Takano, T. Kagayama, T. Nakagawa, M. Takata, and K. Prassides, Phys. Rev. B **80**, 064506 (2009).
- ³⁵ T. Imai, K. Ahilan, F. L. Ning, T. M. McQueen, and R. J. Cava, Phys. Rev. Lett. **102**, 177005 (2009).
- ³⁶ S. Medvedev, T. M. McQueen, I. A. Troyan, T. Palasyuk, M. I. Erements, R. J. Cava, S. Naghavi, F. Casper, V. Ksenofontov, G. Wortmann, and C. Felser, Nat. Mater. **8**, 630 (2009).
- ³⁷ L. Li, Z. Yang, M. Ge, L. Pi, J. Xu, B. Wang, Y. Sun, and Y. Zhang, J Supercond Novel Mag **22**, 667 (2009).
- ³⁸ D. Braithwaite, B. Salce, G. Lapertot, F. Bourdarot, C. Martin, D. Aoki, , and M. Hanflan, J. Phys: Condens. Matter **21**, 232202 (2009).
- ³⁹ G. Garbarino, A. Sow, P. Lejay, A. Sulpice, P. Toulemonde, M. Mezouar, and M. Nunez-Regueiro, Europhys. Lett. **86**, 27001 (2009).
- ⁴⁰ K. Horigane, N. Takeshita, C.-H. Lee, H. Hiraka, and K. Yamada, J. Phys. Soc. Jpn. **78**, 063705 (2009).
- ⁴¹ G. Tsoi, A. Stemshorn, K. Vohra, P. Wu, F. Hsu, Y. Huang, M. Wu, K. Yeh, and S. Weir, J. Phys: Condens. Matter **21**, 232201 (2009).
- ⁴² C.-L. Huang, C.-C. Chou, K.-F. Tseng, Y.-L. Huang, F.-C. Hsu, K.-W. Yeh, M.-K. Wu, and H.-D. Yang, J. Phys. Soc. Jpn. **78**, 084710 (2009).
- ⁴³ A. K. Stemshorn *et al.*, J. Mater. Res. **25**, 396 (2010).
- ⁴⁴ M. H. Fang, H. M. Pham, B. Qian, T. J. Liu, E. K. Vehstedt, Y. Liu, L. Spinu, and Z. Q. Mao, Phys. Rev. B **78**, 224503 (2008).
- ⁴⁵ C. Dong, H. Wang, Z. Li, J. Chen, H. Q. Yuan, and M. Fang, Phys. Rev. B **84**, 224506 (2011).
- ⁴⁶ Y. Kawasaki, K. Deguchi, S. Demura, T. Watanabe,

- H. Okazaki, T. Ozaki, T. Yamaguchi, H. Takeya, and Y. Takano, *Solid State Commun.* **152**, 1135 (2012).
- ⁴⁷ T. Machida, K. Kogure, T. Kato, H. Nakamura, H. Takeya, T. Mochiku, S. Ooi, Y. Mizuguchi, Y. Takano, K. Hirata, and H. Sakata, *Phys. Rev. B* **87**, 214508 (2013).
- ⁴⁸ T. Machida, D. Morohoshi, K. Takimoto, H. Nakamura, H. Takeya, T. Mochiku, S. Ooi, Y. Mizuguchi, Y. Takano, K. Hirata, and H. Sakata, *Physica C* **484**, 19 (2013).
- ⁴⁹ J. Hu, T. J. Liu, B. Qian, and Z. Q. Mao, *Phys. Rev. B* **88**, 094505 (2013).
- ⁵⁰ S. Cao, S. Shen, L. Chen, S. Yuan, B. Kang, and J. Zhang, *J. Appl. Phys.* **110**, 033914 (2011).
- ⁵¹ A. Taraphder and P. Coleman, *Phys. Rev. Lett.* **66**, 2814 (1991).
- ⁵² D. C. Ralph and R. A. Buhrman, *Phys. Rev. Lett.* **69**, 2118 (1992).
- ⁵³ P. W. Anderson, E. Abrahams, and T. V. Ramakrishnan, *Phys. Rev. Lett.* **43**, 718 (1979).
- ⁵⁴ G. J. Dolan and D. D. Osheroff, *Phys. Rev. Lett.* **43**, 721 (1979).
- ⁵⁵ B. Sacepe, C. Chapelier, T. I. Baturina, V. M. Vinokur, and M. R. B. M. Sanquer, *Nat Commun* **1**, 140 (2010).
- ⁵⁶ P. A. Lee, N. Nagaosa, and X.-G. Wen, *Rev. Mod. Phys.* **78**, 17 (2006).
- ⁵⁷ J. B. Ketterson and S. N. Song, *Superconductivity* (Cambridge University Press, 1999).
- ⁵⁸ A. J. Williams, T. M. McQueen, V. Ksenofontov, C. Felser, and R. J. Cava, *J. Phys.: Condens. Matter* **21**, 305701 (2009).